

# Nonanalytic Fermi-liquid correction to the specific heat of RuO<sub>2</sub>

Shubhankar Paul,<sup>1,2,3</sup> Atsutoshi Ikeda,<sup>2</sup> Hisakazu Matsuki,<sup>4</sup> Giordano Mattoni,<sup>1</sup>  
Jörg Schmalian,<sup>5</sup> Chanchal Sow,<sup>3</sup> Shingo Yonezawa,<sup>2</sup> and Yoshiteru Maeno<sup>1</sup>

<sup>1</sup>*Toyota Riken-Kyoto University Research Center (TRiKUC), Kyoto 606-8501, Japan*

<sup>2</sup>*Department of Electronic Science and Engineering,*

*Graduate School of Engineering, Kyoto University, Kyoto 615-8510, Japan*

<sup>3</sup>*Department of Physics, Indian Institute of Technology Kanpur, Kanpur 208016, India*

<sup>4</sup>*Institute for Chemical Research, Kyoto University, Uji, Kyoto 611-0011, Japan*

<sup>5</sup>*Institute for Theory of Condensed Matter and Institute for Quantum Materials and Technologies,  
Karlsruhe Institute of Technology, Karlsruhe 76131, Germany*

(Dated: December 4, 2025)

The magnetic nature of the altermagnet candidate RuO<sub>2</sub> remains under debate. It has been recently shown from quantum oscillations and angle-resolved photoemission spectroscopy (ARPES) that the high-quality RuO<sub>2</sub> bulk single crystal is a paramagnetic metal. However, the low-temperature specific heat exhibits a clear deviation from the conventional  $C(T) = \gamma T + \beta T^3$  dependence; it is well described with nonanalytic Fermi-liquid correction for a clean paramagnetic metal:  $C(T) = \gamma T + \beta T^3 + \delta T^3 \ln(T/T^*)$ . Correspondingly, the magnetic susceptibility is well fitted with the inclusion of  $T^2 \ln T$  term as well as  $H^2 \ln H$  term. In contrast to the spin fluctuation mechanism applicable to some heavy-electron compounds with positive  $\delta$ , RuO<sub>2</sub> shows negative  $\delta$  suggesting a different origin. The observation of such nonanalytic Fermi liquid corrections is attributable to the availability of an ultra-clean sample. The electronic specific heat, the magnetic susceptibility, and the  $T^2$  coefficient in resistivity point to a weakly-correlated 3D Fermi-liquid state with a modest electron correlation, as supported by the Wilson and Kadowaki-Woods ratios.

## I. INTRODUCTION

Ruthenium dioxide RuO<sub>2</sub> in the rutile structure has provided a wide variety of scientific as well as technological interests. It is known as a Pauli paramagnetic metal since 1930s [1–5]. However, fitting of the specific heat with a conventional  $T^3$  term had led to an unusually high Debye temperature [4, 6] due to low-frequency optical phonons with frequencies overlapping with acoustic phonons. With glassy impurities, it is used as a thermometer with small magnetoresistance at low temperatures [7, 8]. It is also well known as a catalyst for the oxygen evolution reaction (OER) [9, 10]. Recently, superconductivity was induced under anisotropic strain [11] and reproduced well in the following study [12].

In 2017, an antiferromagnetic (AFM) ordering with a small room-temperature magnetic moment of approximately  $0.05\mu_B$  ( $\mu_B$  is the Bohr magneton) was reported from polarized neutron diffraction [13]. The AFM ordering with the Néel temperature  $T_N > 300$  K was confirmed with resonant x-ray scattering [14] and angle-resolved photoemission spectroscopy (ARPES) [15]. However, more recent studies with  $\mu$ SR [16], neutron diffraction [17], as well as ARPES [18] did not detect evidence for AFM ordered state.

The issue of intrinsic magnetic properties is particularly important since RuO<sub>2</sub> is considered among the most promising candidate materials of altermagnetism with a large exchange-splitting energy [19, 20]. This novel magnetic state in a certain class of AFM was studied previously [21] and more recent studies of spin splitting, spin-current generation, and anomalous Hall effect [22–25] prepared the stage for the recognition as altermag-

netism. The observed anomalous zero-field Hall effect and spin-torque effect in thin films of RuO<sub>2</sub> are interpreted in terms of altermagnetism [26, 27]. Using ultra-clean crystals [28], we demonstrated by ARPES [18] and quantum oscillations [29] that bulk RuO<sub>2</sub> is paramagnetic down to low temperatures. Nevertheless, the paramagnetic state of RuO<sub>2</sub> deserves special attention as we report in this article.

The low-temperature properties of a paramagnetic metal are well described as a Fermi liquid [30]. It is widely understood that the dominant temperature dependence of thermodynamic quantities in an interacting fermion system is similar to that of non-interacting fermions, but with renormalized parameters. The specific heat at low temperatures is approximated with a combination of the electronic contribution proportional to temperature  $T$  and the phonon contribution proportional to  $T^3$ . However, the next-order corrections may differ significantly from those in non-interacting fermions [31]. Instead of a  $T^3$  correction in the specific heat expected from the Sommerfeld expansion in powers of  $T^2$  for a non-interacting system, a “nonanalytic”  $T^3 \ln T$  term is expected to emerge in three dimensions (3D) due to an intrinsic Fermi-liquid effect [32]. It remains a challenge to find an itinerant electron system that demonstrates the intrinsic Fermi-liquid corrections. Table I compares these analytic and nonanalytic contributions anticipated in specific heat and magnetic susceptibility of Fermi liquids.

We report here that the highly conductive paramagnetic metal RuO<sub>2</sub> exhibits a strong deviation from a simple Fermi-liquid behavior, and the additional nonanalytic term  $T^3 \ln T$  better describes the observation. This addi-

Table I. Analytic and nonanalytic contributions in specific heat and magnetic susceptibility of Fermi liquids.

	$C_p$	$\chi$
phonon	$\beta T^3 + \beta_5 T^5 + \dots$	—
electron (analytic)	$\gamma T + \gamma_3 T^3 + \dots$	$\chi_0 + a_1/T + a_2 T + \dots$
electron (nonanalytic)	$\gamma T + \delta T^3 \ln\left(\frac{T}{T^*}\right)$	$\chi_0 + \frac{a_1}{T} + a_5 T^2 \ln\left(\frac{T}{T_0}\right) + a_6 H^2 \ln\left(\frac{H}{H_0}\right)$
spin-fluctuation	$\delta > 0$ [32, 33]	—
electron-phonon	$\delta < 0$ [32]	—

tional term is suppressed by the magnetic field isotropically. The magnetic susceptibility also fits well with an additional  $T^2 \ln T$  term. Such behavior is not due to magnetic fluctuations, but possibly due to electron-phonon scattering in the Fermi liquid. To the best of our knowledge, such a nonanalytic Fermi-liquid correction has not been systematically demonstrated in a bulk transition-metal system before.

## II. EXPERIMENTAL METHODS

Single crystals of  $\text{RuO}_2$  were grown using the sublimation transport method [28, 34]. High-purity  $\text{RuO}_2$  powder (99.95%, Rare Metallic Ltd.) was placed in an alumina crucible and heated to  $1250^\circ\text{C}$  under a continuous oxygen flow at  $50 \text{ cm}^3/\text{min}$  and the heater was turned off after 100 hrs. Single crystals formed in the lower temperature region at around  $1000^\circ\text{C}$  and predominantly exhibit the (101) facets. The typical crystal dimensions were approximately  $5 \times 3 \times 1 \sim 2 \text{ mm}^3$  as shown in Fig. 1 (b). The crystal planes were identified using x-ray Laue images as well as diffraction peaks of x-ray diffractometer (XRD). Powder x-ray diffraction was used to confirm the phase purity of the crystals. The lattice parameters at room temperature were determined as  $a = 4.49 \text{ \AA}$  and  $c = 3.11 \text{ \AA}$  [28], consistent with previously reported values [3].

Specific heat was measured using a commercial calorimeter system with a helium-3 refrigerator option (Quantum Design, PPMS). The thermometer was calibrated for each magnetic field used in this study. Magnetization was measured using a superconducting quantum interference device (SQUID) magnetometer (Quantum Design, MPMS-XL). For resistivity measurements, we also used MPMS-XL with a self-designed transport probe.

## III. FERMI-LIQUID CHARACTERISTICS

### A. Resistivity

Figure 1(c) represents the resistivity with the current along the [001] direction, plotted against temperature. The details were described in Ref. [28]. The room-

temperature resistivity of  $36 \mu\Omega\text{-cm}$  is consistent with previous reports [34, 36, 37]. The residual resistivity of  $37 \text{ n}\Omega\text{cm}$  corresponds to the mean free path of  $\sim 0.44 \mu\text{m}$ . The residual resistivity ratio  $\text{RRR} = \rho_{300\text{K}}/\rho_{2\text{K}}$  of 1200 is the highest among those reports, indicating the high quality of the single crystals used in this study. For the present specific heat and magnetization studies, single crystals from the same batch as the ones with RRR up to 1200 were used. We then carried out the fitting for the resistivity over the temperature range from 2 to  $375 \text{ K}$  using Bloch-Grüneisen (BG) and Einstein models. The obtained Debye temperature  $\theta_D = 406 \text{ K}$  and Einstein temperature  $\theta_E = 835 \text{ K}$  [28] agree well with those reported in Ref. [38].

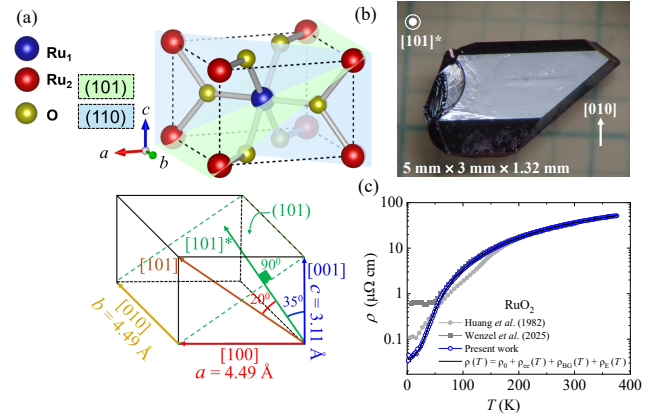


Figure 1. Characterization of  $\text{RuO}_2$  single crystal: (a) Schematic of the rutile crystal structure [35]. In the anticipated antiferromagnetic phase, the Ru sites shown in red (blue) would have magnetic moments up (down) along the [001] direction. The bottom figure shows that the  $[101]^*$  direction, perpendicular the (101) plane, is about 20 degrees different from the [101] direction. (b) Optical image of a typical  $\text{RuO}_2$  single crystal with the size  $5 \times 3 \times 1.3 \text{ mm}^3$ . Crystal orientation is confirmed by x-ray Laue photos. (c) Resistivity with a current along the [001] axis. Needle-shaped crystal elongated along the [001] direction is used [28]. The residual resistivity ratio (RRR) is as large as 1200. The current directions is along the [100] axis for Wenzel *et al.* [36]; but not specified in Huang *et al.* [34].

## B. Specific heat

Figure 2 (a) presents the temperature dependence of the specific heat of RuO<sub>2</sub> single crystals with the RRR of 400 and 1200 at zero field, compared with a previous report. We first attempt the standard fit with a  $T$ -linear electronic term and a Debye  $T^3$ -phonon term:

$$C(T) = \gamma T + \beta T^3. \quad (1)$$

Here  $\gamma$  is the Sommerfeld coefficient, which in the free-electron model is given by:

$$\gamma = \frac{\pi^2 k_B^2 N_A D(\epsilon_F)}{3}, \quad (2)$$

where  $k_B$  is Boltzmann's constant,  $N_A$  is Avogadro's number, and  $D(\epsilon_F)$  is the density of states (DOS) at the Fermi energy that includes both spin directions. If the second term in Eq. (1) contains purely phonon contribution with the Debye temperature  $\theta_D$ ,  $\beta = \beta_{ph}$  given by the following:

$$\beta_{ph} = \frac{12\pi^4 k_B N_A N}{5 \theta_D^3}, \quad (3)$$

where  $N=3$  is the number of atoms in a formula unit for RuO<sub>2</sub>.

The measured specific heat is in reasonable agreement with the literature for a polycrystalline sample down to 0.5 K [4] as well as for a single crystalline sample measured down to 2 K [6]. Nevertheless, the nuclear quadrupole contribution reported in Ref. [4] is absent in our data, consistent with the nuclear magnetic resonance (NMR) measurements [39]. Fitting our zero-field data of RRR=400 crystal using Eq. (1) yields  $\gamma = 5.18 \text{ mJ mol}^{-1}\text{K}^{-2}$ ,  $\beta = 0.0289 \text{ mJ mol}^{-1}\text{K}^{-4}$ , corresponding to  $\theta_D = 587 \text{ K}$ . This is noticeably higher than  $\theta_D \sim 406 \text{ K}$  from the BG fitting of the resistivity. In RuO<sub>2</sub>, a total of 18 vibrational modes are present. Two low-frequency optical phonons have energies comparable to the Debye temperature [40]. Thus,  $\beta_{ph}$  in Eq. (3) properly contains both acoustic and optical phonon excitations at low temperatures.

The specific heat was measured in a magnetic field up to 5 T along the  $[101]^*$  axis parallel to the  $ac$ -plane as shown in Fig. 2 (b). We analysed the data for RRR = 400 in more detail; the data for RRR = 1200 give consistent results as shown in Fig. A1a in appendix A. Although not anticipated in a paramagnetic Fermi liquid, the field-dependent data shown in Fig. A2 in Appendix B deviates significantly from Eq. (1). As shown in Fig. A3, while  $\gamma$  remains constant,  $\beta$  decreases significantly with increasing field. The inclusion of higher-order polynomial terms in  $T$  as in Eq. (19) also leads to unnatural field-dependent phonon terms. Assuming that the phonon contribution remains unaffected by the magnetic field, we attribute such deviation to the electronic contributions including magnetic degrees of freedom.

Next, we considered an analytic expansion for the electronic contribution, including the additional difference between specific heats under constant volume and constant pressure [31]. As examined in Appendix B, the introduction of the electronic  $T^3$  term does not fit the experimental results well. Moreover, in the Fermi gas model, the electronic  $T^3$  term does not depend on the field. Thus, we fit the specific heat with Eq.(4) proposed for a field-dependent nonanalytic correction in a three-dimensional (3D) Fermi liquid [32, 41].

$$C(T, H) = \gamma T + \beta_{ph} T^3 + \delta(H) T^3 \ln \left( \frac{T}{T^*(H)} \right). \quad (4)$$

In fact, the value of  $\gamma$  obtained from Eq. (4) for various fields remains essentially the same. We note that  $T^3 \ln T^*(H)$  term leads to an additional  $T^3$  contribution to the  $\beta T^3$  term:  $\beta = \beta_{ph} - \delta \ln T^*$ . Thus, we fixed the values of  $\gamma$  and  $\beta_{ph}$  to those obtained from the zero-field specific heat and derived the parameters  $\delta(H)$  and  $T^*(H)$ . The zero-field specific heat with Eq. (4) yields  $\gamma$  of  $5.07 \text{ mJ mol}^{-1}\text{K}^{-2}$ . These fitting parameters are presented in Table II, along with those from previous studies on RuO<sub>2</sub>.

The  $T^3 \ln(T/T^*)$  term in specific heat is derived from many-body interactions associated with the multiple scatterings of particle-hole quasiparticle pairs [32, 42]. In such a framework,  $\delta$  is related to the strength of correlations and  $T^*$  is the characteristic temperature of quasiparticle scattering. The characteristic temperature of  $T^* \approx 11 \text{ K}$  is obtained.

We compare the value of  $\gamma$  with the electronic density of states (DOS) at the Fermi energy  $D(\epsilon_F)$  to examine the mass enhancement. From  $\gamma$  and Eq.(2),  $D(\epsilon_F) = 4.294 \text{ states/eV/f.u.} = 29.2 \text{ states/Ry/spin}$ . This value is somewhat higher than  $3.834 \text{ states/eV/f.u.} = 26.07 \text{ states/Ry/spin/f.u.}$  from the band-structure calculation without spin-orbit coupling (SOC) and  $4.067 \text{ states/eV/f.u.} = 27.67 \text{ states/Ry/spin/f.u.}$  including SOC [18]. Here f.u. stands for formula unit. The on-site Coulomb repulsion  $U$  is set to zero in these calculations. The mass enhancement factors are given as follows[43]:

$$\begin{aligned} D(\epsilon_F) &= D_{\text{band}}(1 + \lambda) = D_{\text{FG}} \cdot \frac{m^*}{m} \\ &= D_{\text{FG}} \left( 1 + \frac{F_1^s}{3} \right), \end{aligned} \quad (5)$$

where  $D_{\text{FG}}$  is DOS at  $\epsilon_F$  for a Fermi gas,  $0.662 \text{ states/eV/f.u.}$  for RuO<sub>2</sub>, and  $m^*$  is the effective mass of the electrons. We obtain the enhancement factor  $\lambda = 0.055$  using the calculated value including SOC, and the Landau Fermi-liquid parameter  $F_1^s = 16.5$  from  $\gamma$ . Thus, the mass enhancement  $m^*/m \approx 6.49$  is substantial, but further enhancement over the band mass,  $\lambda$ , is small.

The electronic contribution to the specific heat is presented in Fig. 2 (c) as  $C_{\text{ele}}/T$  plotted against  $T$ :

$$\frac{C_{\text{ele}}(T, H)}{T} = \gamma + \delta(H) T^2 \ln \left( \frac{T}{T^*(H)} \right). \quad (6)$$

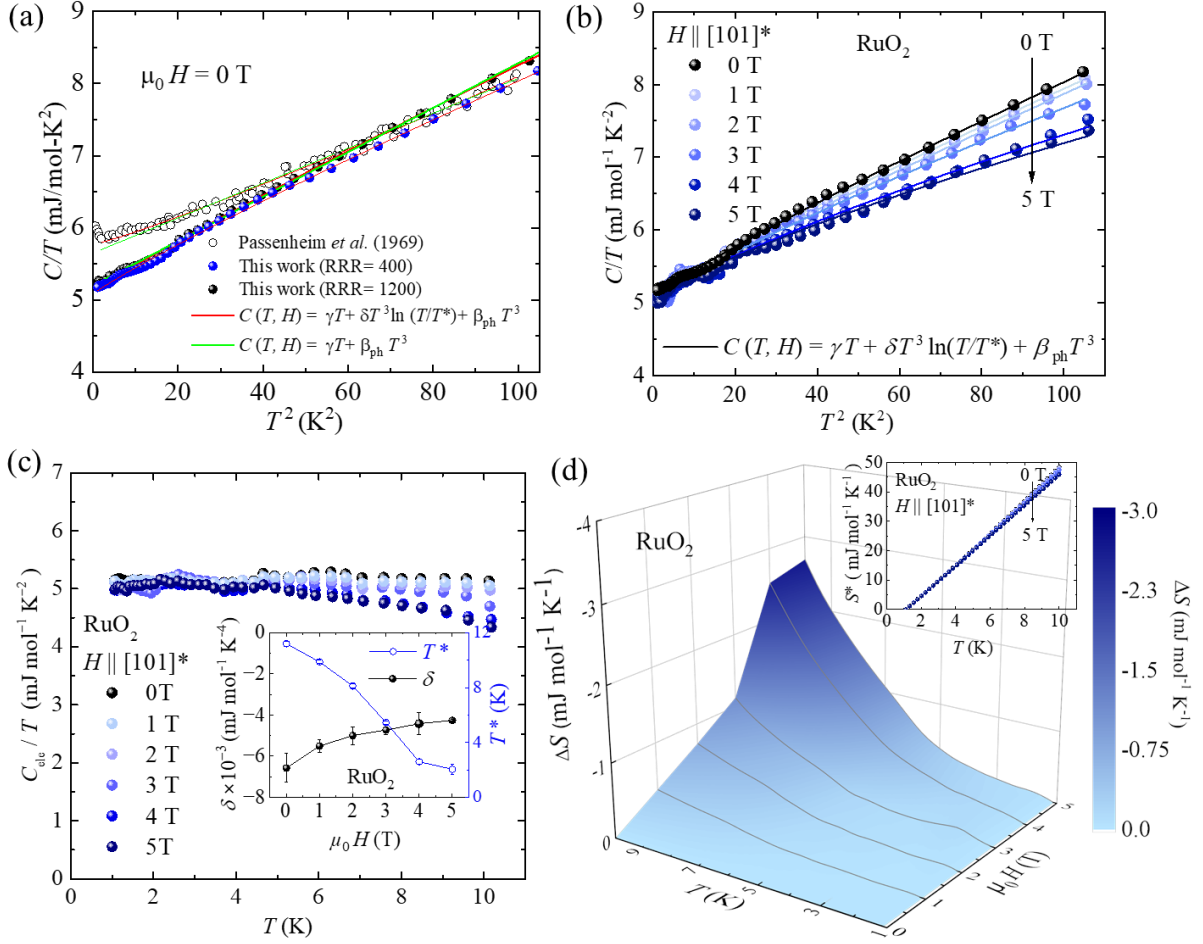


Figure 2. (a) Variations of the zero-field specific heat divided by temperature,  $C/T$ , of a  $\text{RuO}_2$  single crystal measured from 1.1 to 10 K, plotted against  $T^2$ . Experimental data was fitted with both Eq. (1)-(4). The results of the present studies (black sphere) and those of Passenheim and McCollum [4] (open circle) are shown for comparison. (b)  $C/T$  vs  $T^2$  plotted for various fields along with the fitting with Eq. (4). (c) The electronic contribution to the specific heat divided by  $T$ ,  $C_{\text{ele}}/T$ , for various fields. The inset presents the coefficient  $\delta$  and  $T^*$  in Eq. (6) as a function of magnetic field. (d) The temperature dependence of the isothermal entropy change given by Eqs. (7) and (8). Note the negative sign of the vertical axis. The inset shows the entropy increased above  $T_1$ .

We find that the Fermi-liquid correction term becomes larger under field. The inset of Fig. 2 (c) shows the field dependence of the coefficients  $\delta$  and  $T^*$  with magnetic field.

The total entropy  $S(T, H)$  is derived from the specific heat using:

$$\begin{aligned} S(T, H) &= S(T_1, H) + S^*(T, H) \\ &= S(T_1, H) + \int_{T_1}^T \frac{C_{\text{ele}}(T', H)}{T'} dT'. \end{aligned} \quad (7)$$

The first term represents the entropy at the lowest temperature of the measurements,  $T_1 = 1.1$  K in this study, while the second term  $S^*(T, H)$  corresponds to the entropy increase above  $T_1$ , as shown in the inset of Fig.

2(d). Figure 2(d) shows the variation of the entropy with temperature and field:

$$\Delta S(T, H) = S^*(T, H) - S^*(T, H = 0) \quad (8)$$

Reflecting the decrease in entropy with increasing field,  $\Delta S$  becomes more negative. A pronounced magnetocaloric effect is observed, reaching  $-2.6$  mJ/mol·K in a 5 T magnetic field at 10 K. We note that magnetic field dependence is isotropic as shown in Fig. A4 in Appendix C, as expected from Pauli paramagnetic metal.



Table II. Comparison of the fitting parameters for specific heat of RuO<sub>2</sub>. The fitting parameters are derived using Eq.(4) for our work and Eq.(1) for previous reports [4, 6].

parameters	single crystal (this work)	single crystal (this work)	single crystal [6]	polycrystals [4]
RRR	400	1200	500	–
sample mass	36.4 mg	48.1 mg	59.1 mg	18.74 g
$\gamma$ (mJ mol <sup>-1</sup> K <sup>-2</sup> )	5.07	5.12	5.20	5.77
$\beta_{\text{ph}}$ (mJ mol <sup>-1</sup> K <sup>-4</sup> )	0.0289	0.0317	0.0376	0.0225
$\theta_{\text{D}}$ (K)	587	569	544	637
$D(\epsilon_{\text{F}})$ (cell spin Ryd) <sup>-1</sup>	29.2	29.5	30.0	33.2

### C. Magnetization

Here we examine the corresponding nonanalytic effects in magnetization. Figure 3 (a) represents the DC susceptibility, the magnetization  $M$  divided by  $H$ , as a function of temperature up to 200 K under various magnetic fields applied along the [101]\* direction. The inset illustrates the  $M/H$  vs  $T$  up to 400 K; no signature of a magnetic phase transition is observed. Below about 30 K,  $M/H$  increases with decreasing temperature. We note that the observed decrease in the specific heat with magnetic field requires that the intrinsic magnetization decreases with increasing temperature, according to the thermodynamic Maxwell relation:

$$\left(\frac{\partial S}{\partial H}\right)_T = \left(\frac{\partial M}{\partial T}\right)_H. \quad (9)$$

We compare the observed magnetization with the thermodynamic expectation from the Maxwell relation. At 4 K and 2 T, the values of  $\left(\frac{\partial S}{\partial H}\right)_T$  and  $\left(\frac{\partial M}{\partial T}\right)_H$  are estimated to be  $-0.03$  and  $-0.045$  emu-K/mol-T, respectively, suggesting that both intrinsic contribution and paramagnetic-impurity contribution are important. Since it is difficult to deduce the temperature dependence of the intrinsic term from the specific heat, we fit the low-temperature upturn in magnetization using the Curie law equation. For a spin-1 impurity with concentration  $x$ , such as a localized Ru<sup>4+</sup> ion, the expected Curie-term is given as  $a_1 = (g\mu_{\text{B}})^2 S(S+1)x/3k_{\text{B}} = 0.5x$  emu-K/mol. From the fitting of the data for RRR = 400 with Eq. (10) below, we obtain  $a_1 = 1.8 \times 10^{-5}$  emu-K/mol, which corresponds to the impurity concentration of  $x = 36$  ppm [28]. This gives the upper limit of the paramagnetic-impurity concentration. For comparison, Curie-terms in low temperature magnetization reported from different groups somewhat differ: the ratios  $M(2 \text{ K})/M(20 \text{ K})$  (and the RRR values) are 1.08 (400) and 1.01 (1200) in the present work, 1.13 (158) in Ref. [17], and 1.84 (118) in Ref. [36].

For another source of temperature dependence, the DC susceptibility weakly decreases with decreasing temperature from 400 K, as shown in Fig. 3 (a). To express the behaviour at low temperatures, we introduce Eqs. (10) to fit the data as shown in Fig. 3 (b). Adding various

higher-order polynomial terms in  $T$  (such as Eq. (11)) does not improve the fitting.

$$\chi(T, H) = \chi_0 + \frac{a_1}{T} + a_2(H) T, \quad (10)$$

$$\chi(T, H) = \chi_0 + \frac{a_1}{T} + a_3(H) T^2, \quad (11)$$

Corresponding to the nonanalytic term introduced for the specific heat, we include the  $T^2 \ln T$  term given in Eq. (12), predicted for the nonanalytic Fermi-liquid correction [32],

$$\chi(T, H) = \chi_0 + \frac{a_1}{T} + a_4(H) T^2 \ln \left( \frac{T}{T_0(H)} \right). \quad (12)$$

Here,  $\chi_0$  represents the temperature-independent Pauli susceptibility, while  $a_1$  accounts for the Curie-law impurity contribution. The zero-temperature Pauli susceptibility of RuO<sub>2</sub>, obtained from Eq. (12) at 5 T, is  $\chi_0 = 1.58 \times 10^{-4}$  emu/mol =  $1.984 \times 10^{-9}$  m<sup>3</sup>/mol =  $5.77 \times 10^{-5}$  in the electromagnetic unit (EMU) and SI units, which are consistent with previous reports [13, 36]. The Fermi-liquid parameter  $F_0^a$  is defined as follows [43]:

$$\chi_0 = \frac{\chi_{\text{FG}}}{1 + F_0^a}, \quad \chi_{\text{FG}} = \mu_0 \mu_{\text{B}}^2 D_{\text{FG}}. \quad (13)$$

Using the Pauli susceptibility for the Fermi-gas model  $\chi_{\text{FG}} = 0.878 \times 10^{-5}$ , we obtain  $F_0^a = -0.867$ . In Table III, the Landau Fermi liquid parameters  $F_1^s$ ,  $F_0^a$  and other parameters of RuO<sub>2</sub> are compared with those in UPt<sub>3</sub> and <sup>3</sup>He. The magnetization curves at various temperatures from 1.8 K to 400 K are shown in Fig. A5 in Appendix D. These  $M$ - $H$  curves exhibit no hysteresis, consistent with a paramagnetic state. The slope  $M/H$  is temperature and field-dependent, as shown in Fig. 3. Additionally, weak magnetic anisotropy of about 15% is observed when the magnetic field is applied along different crystalline directions as shown in Fig. 3 (c): with 2-T field along the [101]\*,  $[-101]$  and  $[010]$  directions at 2 K,  $\chi_{[101]^*} = 1.75$ ,  $\chi_{[-101]} = 1.55$ , and  $\chi_{[010]} = 1.50 \times 10^{-4}$  emu/mol, respectively. This anisotropic behavior is consistent with previous results [3, 13, 17], but in contrast

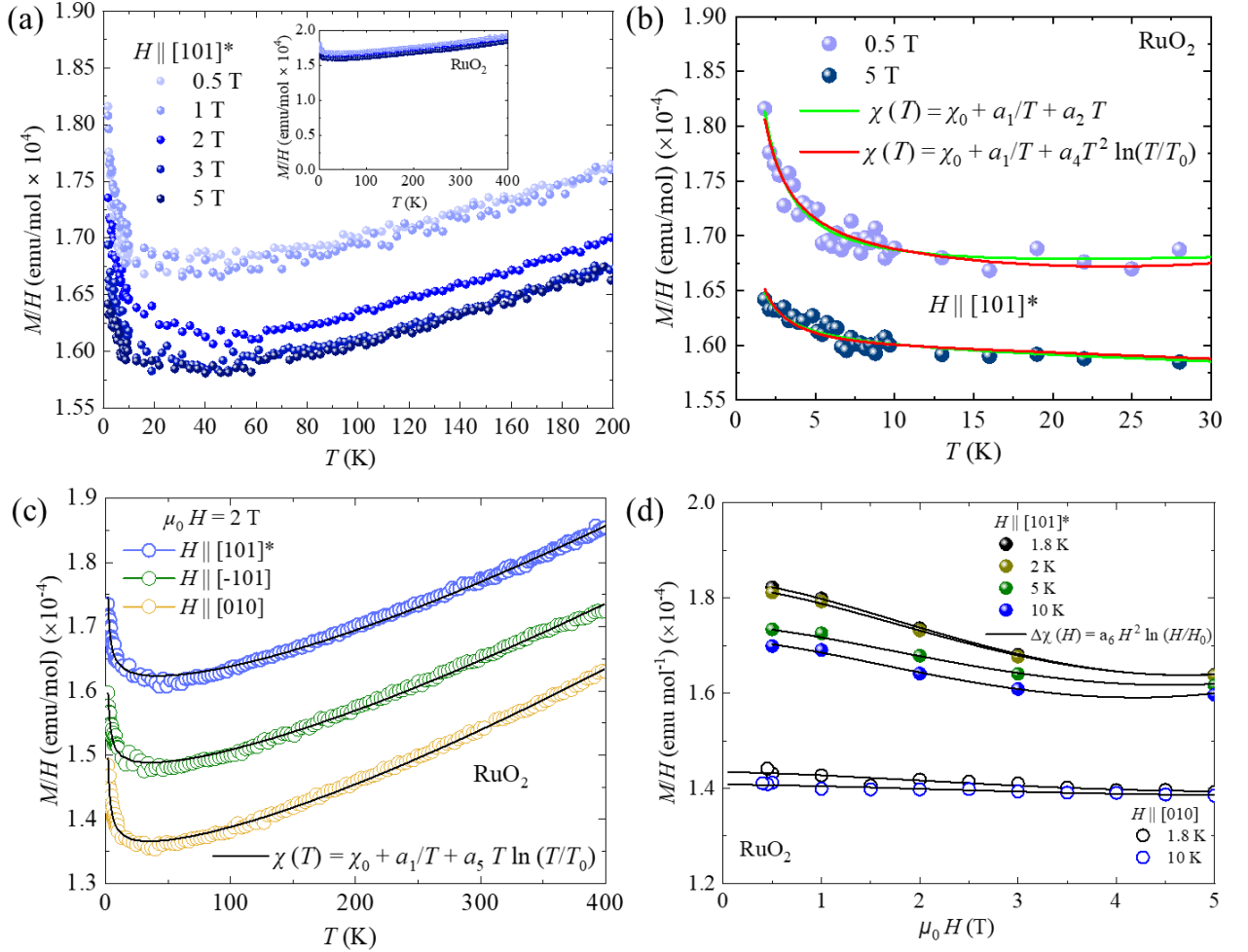


Figure 3. (a) Variation of the DC magnetic susceptibility,  $M/H$ , of RuO<sub>2</sub> with temperature from 1.8 K to 200 K under various magnetic fields  $\mu_0 H$  applied perpendicular to the (101) plane. The inset shows the susceptibility over a broader temperature range (1.8-400 K), revealing no signs of a magnetic transition. (b)  $M/H$  at 0.5 and 5 T fitted by Eqs. (10) and (12). (c) Anisotropy of  $M/H$  at 2 T along different field directions,  $[101]^*$ ,  $[010]$ , and  $[-101]$ . The susceptibility is well fitted with  $T \ln(T/T_0)$  over a wide temperature range. (d) Variation of the DC susceptibility with field at various temperatures up to 10 K. The susceptibility is fitted with  $\Delta\chi(H) = \eta H^2 \ln(H/H_0)$  (Eq. 15), predicted for the Fermi-liquid correction. The data for  $H \parallel [101]^*$  is taken from  $M/H$  vs  $T$  in Fig. 3 (a);  $H \parallel [010]$  from  $M$  vs  $H$  in Fig. A5

with isotropic response of the specific heat under fields shown in Fig. A4 in Appendix C. The nearly parallel shift for different field directions suggests that the anisotropy mainly comes from the  $\chi_0$  term. Considering the highly isotropic specific heat under field, we attribute such modest anisotropy in  $\chi_0$  to the anisotropy of the magnetic enhancement factor. Now we describe the field dependence of the DC susceptibility; as shown in Fig. 3 (a), it decreases with increasing field. Based on the nonanalytic Fermi-liquid behaviour of the specific heat, we introduce the expected temperature- and field-dependent susceptibility in the same framework [32]:

$$\chi(T, H) = \chi_0 + \frac{a_1}{T} + a_5(H=0) T^2 \ln\left(\frac{T}{T_0(H=0)}\right) + \Delta\chi(H), \quad (14)$$

where

$$\Delta\chi(H) = a_6 H^2 \ln\left(\frac{H}{H_0}\right). \quad (15)$$

As shown in Fig. 3(d), the characteristic field obtained from this fitting is  $\mu_0 H_0(T) = 7.7$  T for  $H \parallel [101]^*$  and 8.5 T for  $H \parallel [010]$ . We note that DC susceptibility in

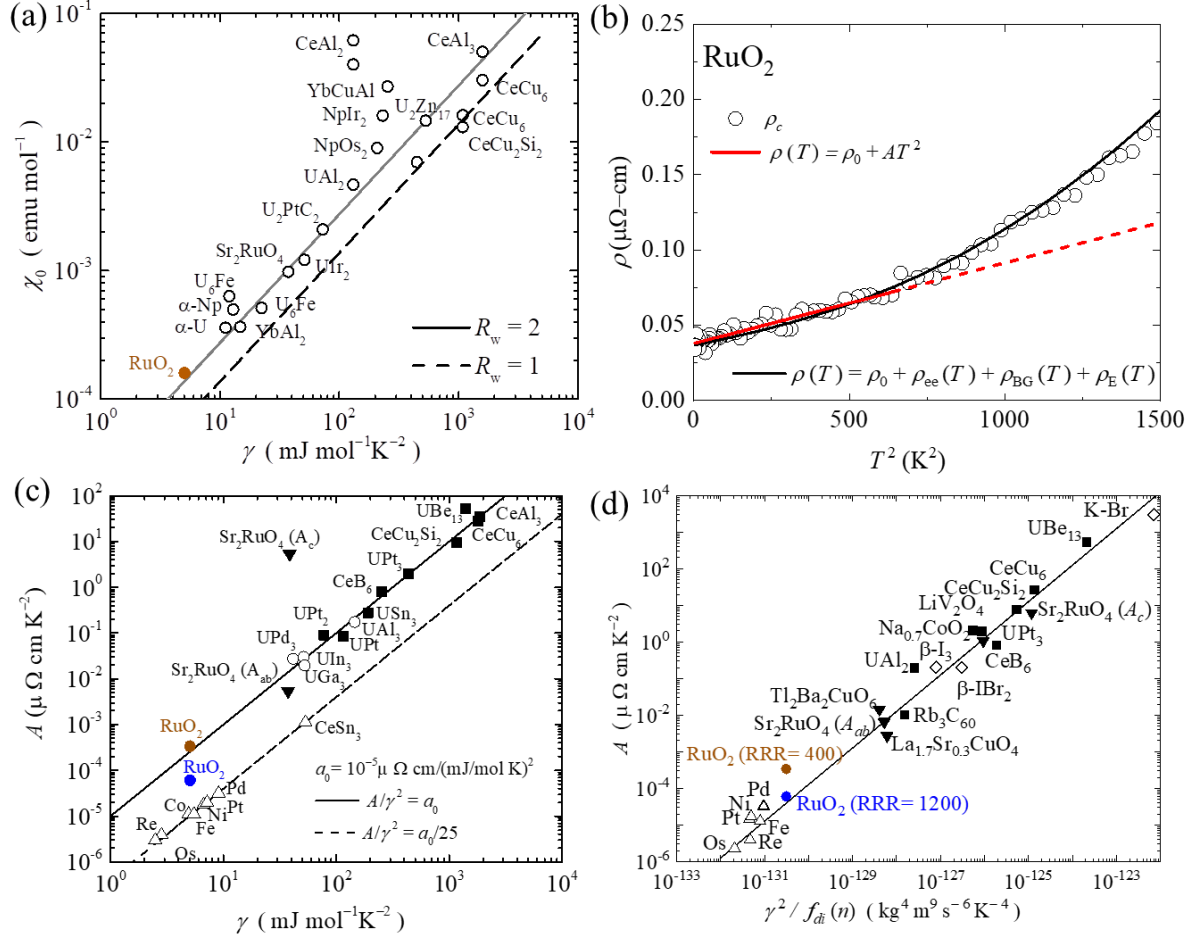


Figure 4. (a) Pauli susceptibility  $\chi_0$  in Eq. (14) plotted on a logarithmic scale against the Sommerfeld coefficient  $\gamma$  in the specific heat for various compounds including RuO<sub>2</sub>. The solid and dashed lines represent the Wilson ratio  $R_W$  of 2 and 1, respectively. (b) The electrical resistivity of RuO<sub>2</sub> for current along the [001] direction plotted against  $T^2$ . The solid line represents the fitting below 25 K using  $\rho(T) = \rho_0 + AT^2$  with  $A = 0.053$  nΩ-cm/K<sup>2</sup>. (c) The  $T^2$  resistivity coefficient  $A$  plotted on a logarithmic scale against  $\gamma$ . Solid and dashed lines represents the Kadowaki-Woods ratio (KWR)  $A/\gamma^2 = a_0 = 1.0 \times 10^{-5}$  μΩ-cm/(mJ/mol-K)<sup>2</sup> and  $a_0/25$ , respectively [44]. (d) Plot of the Kadowaki-Woods-Jacko ratio ( $R_{KWJR}$ ) given by Eq. (17) [45] including RuO<sub>2</sub>.

a wider temperature range up to 400 K fits better with  $T \ln(T/T_0)$  instead of  $T^2 \ln(T/T_0)$  term in Eq. (12), as shown in Fig. 3 (c) with black curves.

#### D. Universality plots

To characterize the strength of electronic correlations, the Wilson ratio

$$R_W = \frac{4\pi^2 k_B^2}{3\mu_0 g^2 \mu_B^2} \left( \frac{\chi_0}{\gamma} \right) \quad (16)$$

is widely used. For a free electron gas,  $R_W$  is unity, and it increases up to 2 for strongly correlated materials [46]. Figure 4 (a) presents  $\chi_0$  versus  $\gamma$  for RuO<sub>2</sub> along with

other strongly and weakly correlated electron systems. The Wilson ratio for RuO<sub>2</sub> is found to be 2.29. RuO<sub>2</sub> may not be considered as a strongly correlated material, considering the modest mass enhancement reflected in the small Sommerfeld coefficient  $\gamma = 5.07$  mJ mol<sup>-1</sup>K<sup>-2</sup>, compared with 40 mJ mol<sup>-1</sup>K<sup>-2</sup> for Sr<sub>2</sub>RuO<sub>4</sub> with a similar carrier density, and in the correspondingly small effective mass obtained from quantum oscillations [29]. Magnetization exhibits some anisotropy (Fig. 3 (c)), in contrast to the isotropic specific heat (Fig. A4); such magnetic anisotropy suggests additional magnetic contribution that enhances the Wilson ratio. Recent plasma frequency studies also classify RuO<sub>2</sub> as a weakly correlated paramagnetic metal [36].

Another key parameter for universal characteriza-

tion of quantum materials is the Kadowaki–Woods ratio (KWR) [44], defined as  $R_{\text{KW}} = A/\gamma^2$ , where  $A$  is the coefficient of the  $T^2$  term in resistivity. Strongly-correlated materials empirically follow  $R_{\text{KW}} = a_0 = 10^{-5} \mu\Omega \text{ cm}/(\text{mJ}/\text{mol K})^2$ . The resistivity of  $\text{RuO}_2$  at low temperatures follows  $\rho(T) = \rho_0 + AT^2$ , as shown in Fig. 4(b). The coefficient  $A$ , estimated by fitting the resistivity data below 25 K, is  $0.053 \text{ n}\Omega\text{-cm}/\text{K}^2$ . This value is two orders of magnitude lower than that of  $\text{Sr}_2\text{RuO}_4$  ( $A = 4.5\text{--}7.5 \text{ n}\Omega\text{-cm}/\text{K}^2$ ) [47]. Figure 4 (c) compares the coefficient  $A$  vs  $\gamma$  for  $\text{RuO}_2$  with various strongly and weakly correlated electron systems, including heavy fermion compounds and transition metals. This plot facilitates comparison of the KWR across different materials, highlighting the degree of electronic correlations present. The KWR for  $\text{RuO}_2$  with  $\text{RRR} = 1200$  is estimated to be  $A/\gamma^2 = 0.2a_0$ , consistent with the universal trend. These suggest that  $\text{RuO}_2$  is a weakly correlated system [48]. Aside from anisotropy of a material, a molar volume is not a universal quantity. Thus, a more generalized rescaling of the original KWR plot has been introduced [45, 49]. Jacko *et al.* [45] expressed the ratio which we call  $R_{\text{KWJR}}$ :

$$R_{\text{KWJR}} = \frac{Af_{di}(n)}{\gamma} = \frac{81}{4\pi\hbar^2 k_{\text{B}}^2 e^2}. \quad (17)$$

Here  $f_{di}(n) \equiv nD_0^2 \langle v_{0i} \rangle \xi^2$ ,  $n$  is the density of the conduction electron,  $\langle v_{0i} \rangle$  is the  $k$  space average of the Fermi velocity and  $\xi \approx 1$  [45]. For an isotropic Fermi-liquid of dimension  $d=3$  and the current direction  $i$ ,  $\xi=1$  and  $f_{3i} = [3n^7/(\pi^4\hbar^6)]^{1/3}$ . Using the conduction electron density for  $\text{RuO}_2$  of  $n = 0.129 \times 10^{30} \text{ m}^{-3}$ ,  $\gamma_{\text{RuO}_2} = 5.07 \text{ mJ mol}^{-1} \text{ K}^{-2} = 266 \text{ kg K}^{-2}\text{s}^{-2}\text{m}$ ,  $f_{3i}(n)$  is estimated to be  $2.28 \times 10^{135} \text{ kg}^2\text{m}^{11}\text{s}^{-2}$ . Figure 4(d) compares the  $R_{\text{KWJR}}$  values with other materials. In this plot,  $\text{RuO}_2$  is characterized by an exceptionally low value of  $A$  among oxides and intermetallic compounds.

#### IV. DISCUSSION AND CONCLUSION

The low-temperature specific heat of high-purity  $\text{RuO}_2$  exhibits an unusual magnetic-field dependence; the  $T^3$  term, normally considered as a phonon contribution, depends strongly on the magnetic field. At higher fields, the deviation from the conventional  $\gamma T + \beta T^3$  behavior becomes stronger, although the specific heat decreases isotropically. Such overall deviation is well fitted by non-analytic correction for the Fermi liquid,  $\delta T^3 \ln(T/T^*)$ . Correspondingly, the spin susceptibility also contains the  $T^2 \ln T$  term at low temperatures. Experimentally, this phenomenon was initially observed in the specific heat of liquid  $^3\text{He}$  by Wheatley *et al.* and used to determine its Landau Fermi-liquid parameters [43, 50, 51]. For itinerant electron systems, the nonanalytic  $T^3 \ln T$  term in the specific heat is recognized in some heavy fermion systems such as  $\text{UPt}_3$ , and it is understood as due to spin fluctuations arising from quasiparticle interactions in Fermi

liquids [33]. Nevertheless, the corresponding spin susceptibility does not agree well with the thermodynamic requirement from the specific heat.

The nonanalytic behavior in  $\text{RuO}_2$  is in sharp contrast to the spin fluctuation contribution in heavy-fermion systems [33]. In  $\text{RuO}_2$  the sign of  $\delta$  is negative and  $C/T$  decreases by 9% under the magnetic field of 5 T, whereas in  $\text{UPt}_3$   $\delta$  is positive and  $C/T$  increases at most a few % at 5 T at low temperature [33]. Concerning the origin of nonanalytic corrections, theories predict positive contribution from the electron-phonon scattering and negative contribution from the electron-electron processes including the repeated electron-hole scattering leading to spin fluctuations [32, 42]. The spin susceptibility in  $\text{RuO}_2$  is dominated by a  $T$ -independent Pauli term and exhibits a modest 15% anisotropy, whereas in  $\text{UPt}_3$  it is strongly temperature dependent and anisotropic with different signs of  $(\partial M/\partial T)$ , depending on the field direction.

If the nonanalytic correction is dominated by the electron-phonon process, both  $T^*$  and  $T_0$  are expected to take similar values. An outstanding question is whether the observed characteristic values,  $T^* \approx 11 \text{ K}$  in the specific heat and  $T_0 \approx 30 \text{ K}$  in the spin susceptibility, are consistently explained by the electron-phonon process. The universality plots of the Wilson ratio and the Kadowaki-Woods ratios places  $\text{RuO}_2$  as weakly correlated Fermi liquid. The contrasting behavior of the isotropic specific heat and the weakly anisotropic spin susceptibility of  $\text{RuO}_2$  suggests additional magnetic enhancement that leads to its Wilson ratio being greater than 2.

#### ACKNOWLEDGEMENTS

We are grateful to S. Souma, M. Sato, T. Osumi, K. Yamauchi, A. Eaton, T. Johnson, and A. V. Chubukov for useful discussions. This work was supported by the JSPS KAKENHI (JP22H01168, JP23K22439, JP25K17346) and the JST Sakura Science Exchange Program. C.S. acknowledges research support from IIT Kanpur Initiation Grant (IITK-2019-037) and research grants from Science and Engineering Research Board (SERB), Government of India (SRG2019-001104, CRG-2022-005726, EEQ-2022-000883). G.M. and H.M. acknowledge support from the Kyoto University Foundation. G.M. acknowledges support from the Toyota Riken Scholar Program.

#### APPENDIX

##### A. Field dependent specific heat variation of the $\text{RRR} = 1200$ crystal

Figure A1a presents the field-dependent specific heat for  $\text{RRR} = 1200$ , along with the nonanalytic fit using Eq.



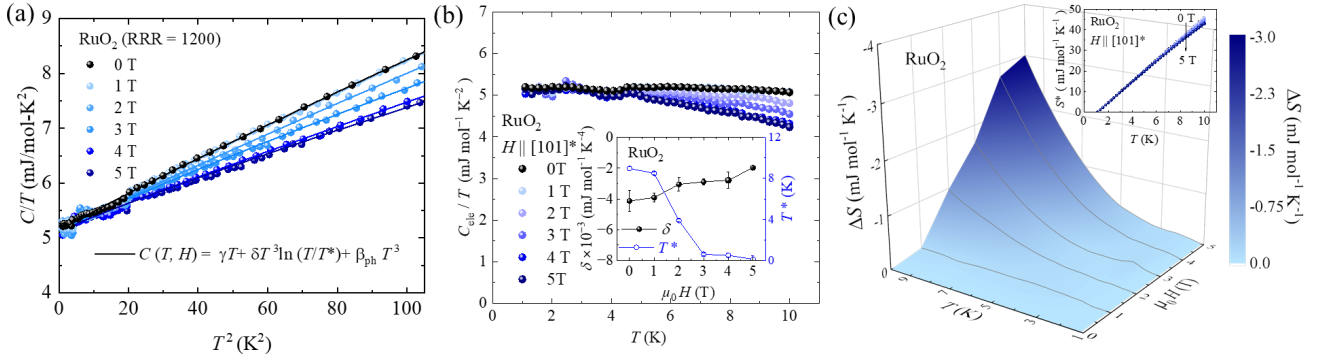


Figure A1. (a)–(c) The thermodynamic analysis of a crystal with RRR = 1200, corresponding to Fig. 2(b)–(d) for a crystal with RRR = 400. (a)  $C/T$  is plotted against  $T^2$  for different magnetic fields, together with the corresponding fits to Eq. 4. (b) The electronic contribution to the specific heat,  $C_{\text{ele}}/T$ , under various fields. The inset shows the field dependence of the parameters  $\delta$  and  $T^*$  obtained from Eq. 4. (c) The temperature dependence of the isothermal entropy change calculated using Eq. (7)–(8). The inset shows the temperature-dependent entropy above  $T_1$ .

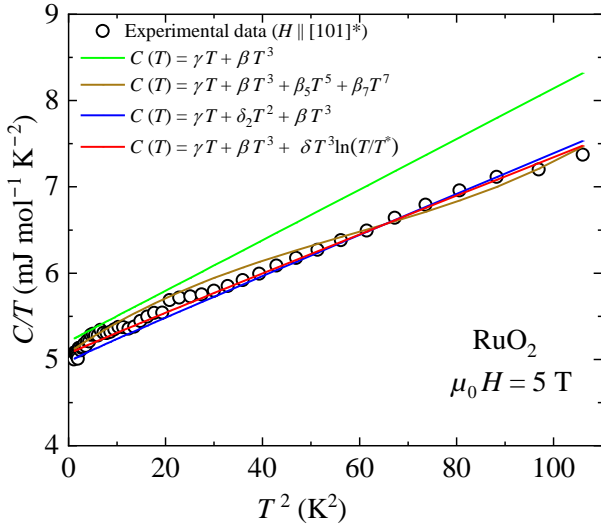


Figure A2. Fitting of the specific heat divided by temperature at 5 T with various functions. The values of  $\gamma$  and  $\beta$  for each fit are kept fixed to the values determined from the zero-field data using the corresponding equation.

4. The field-dependent electronic contribution, obtained from Eq. 6, is shown in Fig. A1b. Figure A1c illustrates the entropy variation as a function of temperature and magnetic field.

### B. Nonanalytic term in the specific heat

Figure A2 shows the specific heat of  $\text{RuO}_2$  divided by temperature under the magnetic field of 5 T along the  $[101]^*$  direction. We fit the data at 5 T in the following expressions containing analytic or nonanalytic correction

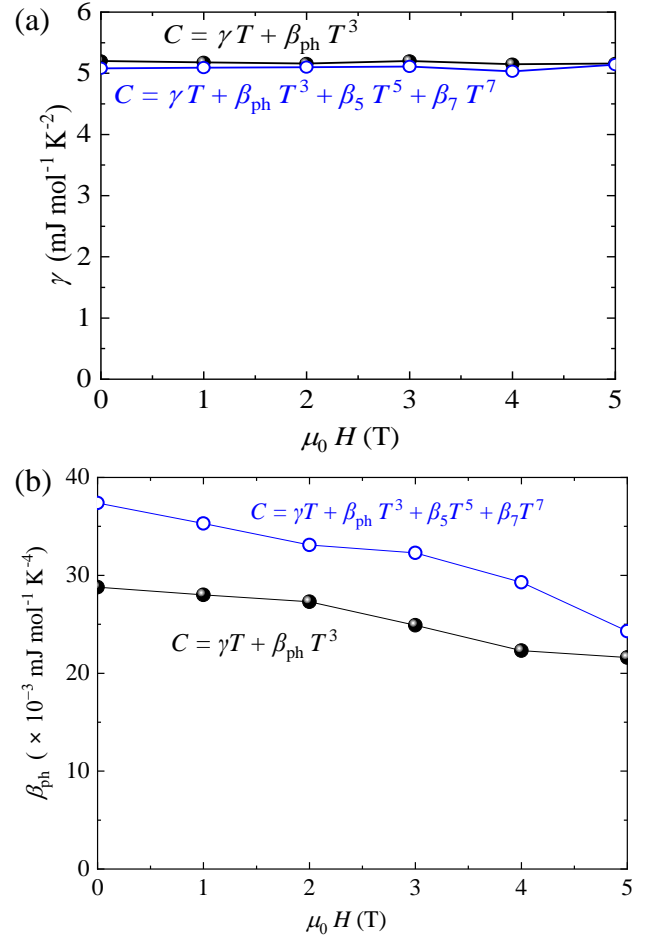


Figure A3. Field dependence of (a)  $\gamma$  and (b)  $\beta$  coefficients when the specific heat results are fitted with Eq. (18) (19).

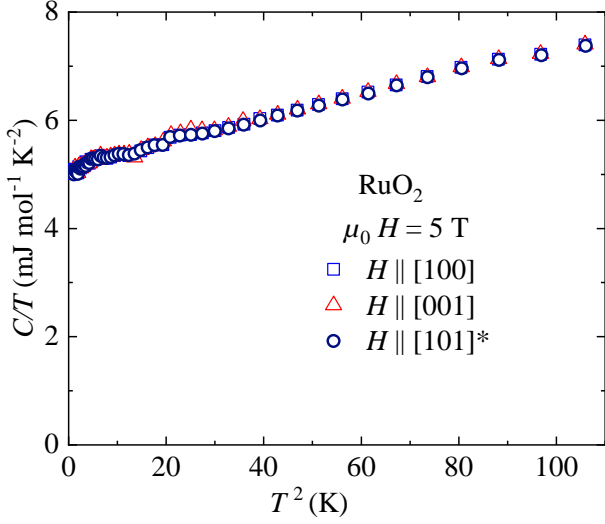


Figure A4. Specific heat of RuO<sub>2</sub> divided by temperature plotted against  $T^2$ , measured from 1.1 to 10 K under the magnetic field of 5 T applied along the [101]\*, [001], and [010] directions. It shows no observable anisotropy.

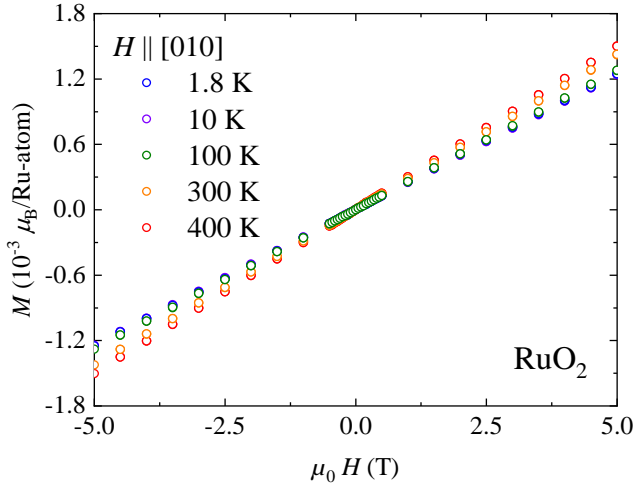


Figure A5. Magnetization vs magnetic field along the [010] direction at various temperatures.

terms:

$$C(T) = \gamma T + \beta T^3, \quad (18)$$

$$C(T, H) = \gamma T + \beta T^3 + \beta_5(H) T^5 + \beta_7(H) T^7, \quad (19)$$

$$C(T, H) = \gamma T + \beta_{\text{ph}} T^3 + \delta(H) T^3 \ln \left( \frac{T}{T^*(H)} \right). \quad (20)$$

To demonstrate what happens to the inclusion of the higher-order polynomial terms in Eq. (18) (19) to fit the data, Fig. A3 shows the variations of  $\gamma$  and  $\beta$  with field. Such field-dependent  $T^3$  term in the specific heat suggests that the electronic contribution is important in addition to the phonon contribution. The values of  $\gamma$  and  $\beta$  for each fit are fixed to the values obtained for the zero-field data using the corresponding equation. In the Fermi gas model, the higher-order analytic correction to Eq. (18) is given by Eq. (19), where  $\beta = \beta_{\text{ph}} + \beta_{\text{ele}}$  [31]:

$$\beta_{\text{ele}} = -\frac{\pi^2 k_B^4 N_A D(\epsilon_F)}{9\epsilon_F^2} \left( \frac{9\pi^2}{20} - 1 \right). \quad (21)$$

The second term in the parentheses is needed to convert  $C_V$  to  $C = C_P$ . As demonstrated in Fig. A4, the fitting with Eq. (21) among these fitting functions provides the best match to the experimental results.

### C. Isotropic field dependence of the specific heat

Figure A4 illustrates the direction-dependent specific heat, measured in the magnetic field of 5 T. To investigate the contribution of spin fluctuations, we applied the magnetic field perpendicular to three crystallographic planes: (100), (001), and (101). In particular, no anisotropy was observed at a field strength of 5 T.

### D. Magnetization curves

The magnetization versus field curves at different temperatures are nearly linear, as shown in Fig. A5. This linear behavior is characteristic of a paramagnetic response.

### E. Comparison of Fermi-liquid parameters

To compare the nonanalytic Fermi-liquid behavior in RuO<sub>2</sub> with those in the heavy-fermion compound UPt<sub>3</sub> and normal liquid <sup>3</sup>He, Table III below summarizes the Landau Fermi-liquid parameters as well as other relevant parameters.

Table III. Comparison of the Fermi-liquid and other parameters of RuO<sub>2</sub> in this work (RRR = 400) with those of the heavy Fermion system UPt<sub>3</sub> [33] and the normal liquid <sup>3</sup>He at ambient pressure [51].

	parameters	RuO <sub>2</sub> (this work)	UPt <sub>3</sub> [33]	<sup>3</sup> He [51]
Effective mass ratio	$m^*/m$	6.265	180	2.76
Landau Fermi-liquid parameter	$F_1^s$	15.8	540	5.27
	$F_0^a$	-0.867	-0.778	-0.700
RRR	$\rho_{300\text{ K}}/\rho_{2\text{ K}}$	400		
Carrier density	$n$ (m <sup>-3</sup> )	$0.128 \times 10^{30}$		
Sommerfeld coefficient	$\gamma$ (mJ mol <sup>-1</sup> K <sup>-2</sup> )	5.07	421	$22.8 \times 10^3$
Phonon $T^3$ contribution	$\beta_{\text{ph}}$ (mJ mol <sup>-1</sup> K <sup>-4</sup> )	0.0289	0.85	—
Electron $T^3$ contribution	$\beta_{\text{ele}} = -\delta \ln T^*$	0.015	-3.72	$-2.39 \times 10^5$
Electron $T^3$ contribution	$\beta_{\text{ele}}$ (Fermi gas)	$-1.52 \times 10^{-10}$		
Quasiparticle interaction	$\delta$ (mJ mol <sup>-1</sup> K <sup>-4</sup> )	$-6.58 \times 10^{-3}$	1.38	$3.06 \times 10^5$
Coupling constant ratio	$\lambda$	0.055	1.3	
Characteristic temperature	$T^*$ (K)	11	27	0.458
Characteristic field	$\mu_0 H_0$ (T)	8.5 ( $H \parallel [010]$ )	-	
Residual resistivity	$\rho_0$ ( $\mu\Omega$ cm)	0.037	6.2	—
Fermi energy (Fermi gas)	$\epsilon_F$ (eV)	9.243		
Density of states (Fermi gas)	$D_0(\epsilon_F)$ (states eV <sup>-1</sup> f.u. <sup>-1</sup> )	0.649		
Density of states (band calc.)	$D_{\text{band}}$ (states eV <sup>-1</sup> f.u. <sup>-1</sup> )	4.067		
Density of states ( $\gamma$ in $C_P$ )	$D_{\text{exp}}$ (states eV <sup>-1</sup> f.u. <sup>-1</sup> )	4.294		

- [1] A. N. Guthrie and L. Bourland, *Physical Review* **37**, 303 (1931).
- [2] W. Ryden and A. Lawson, *The Journal of Chemical Physics* **52**, 6058 (1970).
- [3] W. Ryden, A. Lawson, and C. C. Sartain, *Physical Review B* **1**, 1494 (1970).
- [4] B. Passenheim and D. McCollum, *The Journal of Chemical Physics* **51**, 320 (1969).
- [5] J. Fletcher, W. Gardner, B. Greenfield, M. Holdoway, and M. Rand, *Journal of the Chemical Society A*, 653 (1968).
- [6] M. Mertig, G. Pompe, and E. Hegenbarth, *Physica Status Solidi (b)* **135**, 335 (1986).
- [7] H. Doi, Y. Narahara, Y. Oda, and H. Nagane, in *Proc. LT17, Karlsruhe* (North-Holland, Amsterdam, 1984) p. 405.
- [8] S. A. Myers, H. Li, and G. A. Cs  thy, *Cryogenics* **119**, 103367 (2021).
- [9] H. Over, Y. D. Kim, A. P. Seitsonen, S. Wendt, E. Lundgren, M. Schmid, P. Varga, A. Morgante, and G. Ertl, *Science* **287**, 1474–1476 (2000).
- [10] X. Ping, Y. Liu, L. Zheng, Y. Song, L. Guo, S. Chen, and Z. Wei, *Nature Communications* **15**, 10.1038/s41467-024-46815-6 (2024).
- [11] J. P. Ruf, H. Paik, N. J. Schreiber, H. P. Nair, L. Miao, J. K. Kawasaki, J. N. Nelson, B. D. Faeth, Y. Lee, B. H. Goodge, *et al.*, *Nature Communications* **12**, 59 (2021).
- [12] M. Uchida, T. Nomoto, M. Musashi, R. Arita, and M. Kawasaki, *Physical Review Letters* **125**, 147001 (2020).
- [13] T. Berlijn, P. C. Snijders, O. Delaire, H.-D. Zhou, T. A. Maier, H.-B. Cao, S.-X. Chi, M. Matsuda, Y. Wang, M. R. Koehler, *et al.*, *Physical Review Letters* **118**, 077201 (2017).
- [14] Z. Zhu, J. Stremper, R. Rao, C. Occhialini, J. Pellicciari, Y. Choi, T. Kawaguchi, H. You, J. Mitchell, Y. Shao-Horn, *et al.*, *Physical Review Letters* **122**, 017202 (2019).
- [15] Z. Lin, D. Chen, W. Lu, X. Liang, S. Feng, K. Yamagami, J. Osiecki, M. Leandersson, B. Thiagarajan, J. Liu, C. Felser, and J. Ma, preprint arXiv: 2402.04995 (2024).
- [16] M. Hiraiishi, H. Okabe, A. Koda, R. Kadono, T. Muroi, D. Hirai, and Z. Hiroi, *Physical Review Letters* **132**, 166702 (2024).
- [17] L. Kiefer, F. Wirth, A. Bertin, P. Becker, L. Bohat  y, K. Schmalzl, A. Stunault, J. A. Rodr  guez-Velamaz  n, O. Fabelo, and M. Braden, *Journal of Physics: Condensed Matter* **37**, 135801 (2025).
- [18] T. Osumi, K. Yamauchi, S. Souma, S. Paul, A. Honma, K. Nakayama, K. Ozawa, M. Kitamura, K. Horiba, H. Kumigashira, C. Bigi, F. Bertran, T. Oguchi, T. Takahashi, Y. Maeno, and T. Satoand, preprint arXiv:2501.10649 (2025).
- [19] L.   mejkal, J. Sinova, and T. Jungwirth, *Physical Review X* **12**, 031042 (2022).
- [20] L.   mejkal, J. Sinova, and T. Jungwirth, *Physical Review X* **12**, 040501 (2022).
- [21] Y. Noda, K. Ohno, and S. Nakamura, *Physical Chemistry Chemical Physics* **18**, 13294–13303 (2016).
- [22] K.-H. Ahn, A. Hariki, K.-W. Lee, and J. Kune  , *Physical Review B* **99**, 10.1103/physrevb.99.184432 (2019).
- [23] M. Naka, S. Hayami, H. Kusunose, Y. Yanagi, Y. Motome, and H. Seo, *Nature Communications* **10**, 10.1038/s41467-019-12229-y (2019).

- 
- [24] L. Šmejkal, R. González-Hernández, T. Jungwirth, and J. Sinova, *Science Advances* **6**, eaaz8809 (2020).
  - [25] S. Hayami, Y. Yanagi, and H. Kusunose, *Journal of the Physical Society of Japan* **88**, 10.7566/jpsj.88.123702 (2019).
  - [26] S. Karube, T. Tanaka, D. Sugawara, N. Kadoguchi, M. Kohda, and J. Nitta, *Physical Review Letters* **129**, 137201 (2022).
  - [27] Z. Feng, X. Zhou, L. Šmejkal, L. Wu, Z. Zhu, H. Guo, R. González-Hernández, X. Wang, H. Yan, P. Qin, *et al.*, *Nature Electronics* **5**, 735 (2022).
  - [28] S. Paul, G. Mattoni, H. Matsuki, T. Johnson, C. Sow, S. Yonezawa, and Y. Maeno, *Journal of Crystal Growth*, 128405 (2025).
  - [29] Z. Wu, M. Long, H. Chen, S. Paul, H. Matsuki, O. Zhe-liuk, U. Zeitler, G. Li, R. Zhou, Z. Zhu, *et al.*, *Physical Review X* **15**, 031044 (2025).
  - [30] A. A. Abrikosov, *Fundamentals of the theory of metals* (Dover, 1988).
  - [31] N. W. Ashcroft and N. D. Mermin, *Solid State Physics* (Holt, Rinehart and Winston, 1976).
  - [32] A. V. Chubukov, D. L. Maslov, and A. J. Millis, *Physical Review B* **73**, 045128 (2006).
  - [33] A. De Visser, A. Menovsky, and J. Franse, *Physica B+C* **147**, 81–160 (1987).
  - [34] Y. Huang, H. Park, and F. H. Pollak, *Materials Research Bulletin* **17**, 1305 (1982).
  - [35] K. Momma and F. Izumi, *Applied Crystallography* **41**, 653 (2008).
  - [36] M. Wenzel, E. Uykur, S. Rößler, M. Schmidt, O. Janson, A. Tiwari, M. Dressel, and A. A. Tsirlin, *Physical Review B* **111**, L041115 (2025).
  - [37] F. Pawula, A. Fakih, R. Daou, S. Hébert, N. Mordvinova, O. Lebedev, D. Pelloquin, and A. Maignan, *Physical Review B* **110**, 064432 (2024).
  - [38] J.-J. Lin, S. Huang, Y. Lin, T. Lee, H. Liu, X. Zhang, R. Chen, and Y. Huang, *Journal of Physics: Condensed Matter* **16**, 8035 (2004).
  - [39] H. Mukuda, K. Ishida, Y. Kitaoka, K. Asayama, R. Kanno, and M. Takano, *Physical Review B* **60**, 12279 (1999).
  - [40] K.-P. Bohnen, R. Heid, O. d. l. P. Seaman, B. Renker, P. Adelmann, and H. Schober, *Physical Review B* **75**, 10.1103/physrevb.75.092301 (2007).
  - [41] H. Van Der Meulen, Z. Tarnawski, J. Franse, and J. Perenboom, *Physica B* **163**, 385 (1990).
  - [42] D. Coffey and C. J. Pethick, *Physical Review B* **33**, 7508–7513 (1986).
  - [43] D. Vollhardt and P. Wölfle, *The Superfluid Phases of Helium 3* (Taylor & Francis, 1990).
  - [44] K. Kadowaki and S. Woods, *Solid State Communications* **58**, 507 (1986).
  - [45] A. C. Jacko, J. O. Fjærestad, and B. J. Powell, *Nature Physics* **5**, 422–425 (2009).
  - [46] J. R. Engelbrecht and K. S. Bedell, *Physical Review Letters* **74**, 4265–4268 (1995).
  - [47] Y. Maeno, K. Yoshida, H. Hashimoto, S. Nishizaki, S.-i. Ikeda, M. Nohara, T. Fujita, A. P. Mackenzie, N. E. Hussey, J. G. Bednorz, *et al.*, *Journal of the Physical Society of Japan* **66**, 1405 (1997).
  - [48] Y. Ling, F. Pawula, R. Daou, B. Fauque, and K. Behnia, *arXiv preprint arXiv:2511.04278* (2025).
  - [49] N. E. Hussey, *Journal of the Physical Society of Japan* **74**, 1107–1110 (2005).
  - [50] W. R. Abel, A. C. Anderson, W. C. Black, and J. C. Wheatley, *Physical Review* **147**, 111–119 (1966).
  - [51] D. S. Greywall, *Physical Review B* **27**, 2747 (1983).